

Soft X-ray Lithography with a Monomolecular Resist

The recent technological trend toward molecular electronics, biochips, templates for molecular recognition, and cell receptors requires novel approaches for the fabrication of chemical and biological submicron- and nano-structures. Perspective materials to provide the basis for the respective technology are self-assembled monolayers (SAMs), which are well-ordered and densely packed 2D-ensembles of chain-like organic molecules anchored to a substrate by a suitable headgroup. SAMs can be modified by electron irradiation or some other means, including a chemical transformation of the functional tail group at the end of the molecular chain, which can then be used as a linker to couple even more complex entities to the surface. The tailored character of the modification, the monolayer thickness of the film, and the molecular size of its structural elements make SAMs to suitable resist materials and an ideal platform for the fabrication of micro- and nano-structures. Applying proximity printing or direct-writing, "conventional" and chemical lithographic patterns and templates could be formed. Recently the patterning has reached nanometer length scale with advanced experimental tools such as highly-focused electron beam and scanning probe microscope tip.

Pattern fabrication using an electron beam is especially attractive because of the well-established setups from conventional electron lithography and a detailed knowledge of the physical and chemical changes induced by the irradiation. Spectroscopic analysis of the complex phenomena involved in the interactions of electrons with SAMs showed that the two major competitive processes taking place in the reaction are decomposition/desorption of the film and cross-linking of neighboring moieties. Whereas the former process is the dominant effect for the aliphatic SAMs (which results in a rather

disordered, physisorbed layer), quasi-polymerization occurs in aromatic films and greatly reduces the damage of the system. Keeping such a film intact, one can also modify the functional tail group, creating a new chemical identity of the film surface or a surface area.

The concept developed for the e-beam lithography with a SAM resist can be directly transferred to X-ray lithography, considering that the major impact of X-ray irradiation is provided by photoelectrons and inelastic secondary electrons. We applied a focused soft X-ray beam for direct lithographic writing in a SAM resist, provided by the Fresnel zone plate optics, which is a part of the scanning photoelectron microscopy (SPEM) station at U5 beamline. The experimental setup allows both the fabrication and characterization of the lithographic patterns by raster-scanning the sample with respect to the X-ray beam and collecting the emitted photoelectrons at each point.

Three different kinds of SAMs on Au substrates were used as test systems, namely conventional, non-substituted and semifluorinated aliphatic SAMs, $\text{CH}_3(\text{CH}_2)_{15}\text{SH}$ and $\text{CF}_3(\text{CF}_2)_9(\text{CH}_2)_{11}\text{SH}$ (abbreviated as C16 and F10H11, respectively) and an aromatic monolayer of nitrophenylthiolate $\text{NO}_2(\text{C}_6\text{H}_4)_2\text{SH}$ (abbreviated as NBPT). The photon energy was set at 387 eV, close to the efficiency maximum of the zone plate optics. Whereas the spatial resolution of the SPEM setup is about 200 nm, a larger pixel width of 500 nm has been used for the writing. The writing was carried out by scanning areas of rectangular shape with the focused beam using an irradiation time per pixel of 90 ms. This was followed by scanning a larger area ($70\ \mu\text{m} \times 70\ \mu\text{m}$) with dwell time of 60 ms and pixel width of 700 nm for taking the photoelectron images of the patterned surface.

Figure 1 shows the Au $4f_{7/2}$ and C 1s SPEM

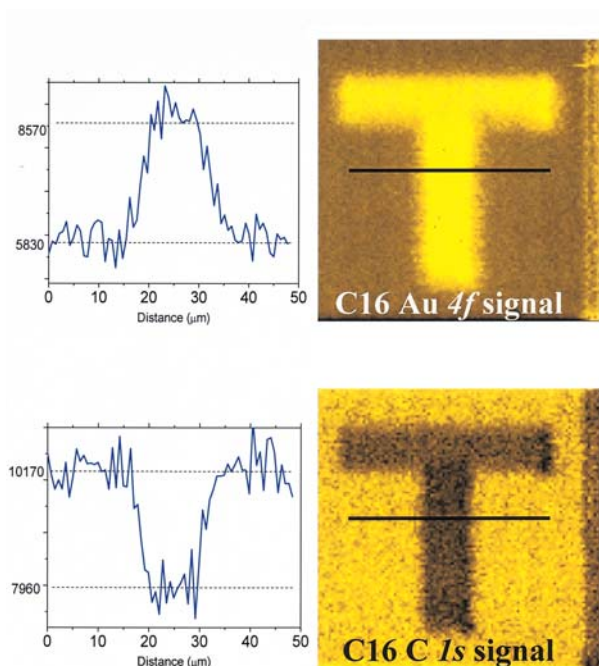


Fig. 1: Au $4f_{7/2}$ and C $1s$ SPEM images (image size $70 \times 70 \mu\text{m}^2$) of soft X-ray microbeam patterned C16/Au taken at a photon energy (PE) of 387 eV. The intensity profiles are taken along the lines as indicated in the images. A stripe of damaged area at the right end of the images stems from a longer (some milliseconds) stay of the focused beam at the end of each line scan.

images of an X-ray microbeam pattern (letter "T") in C16 resist. Below the images are the corresponding intensity profiles taken across the solid lines. In the Au $4f_{7/2}$ image, the intensity from the irradiated area is by $\approx 47\%$ higher than that from the non-irradiated one, whereas the inverse intensity relation with an intensity difference of $\approx 22\%$ is observed for the C $1s$ image. This is caused by the irradiation-induced desorption of the molecular fragments from the irradiated area, similar to the case of electron irradiation.

A second example of X-ray microprobe writing is F10H11/Au. This film is composed of a hydrocarbon part attached to the substrate and a fluorocarbon part forming the SAM-ambient interface. The C $1s$ XPS spectrum of the pristine film exhibits three distinct emissions corresponding to the CH_2 , CF_2 , and CF_3 moieties, as shown in Fig. 2 (bottom spectrum). The emission from the hydrocarbon chain is much smaller as compared to that for the fluorocarbon part due to a strong suppression of the respective signal by the fluorocarbon overlayer; the mean free path for the

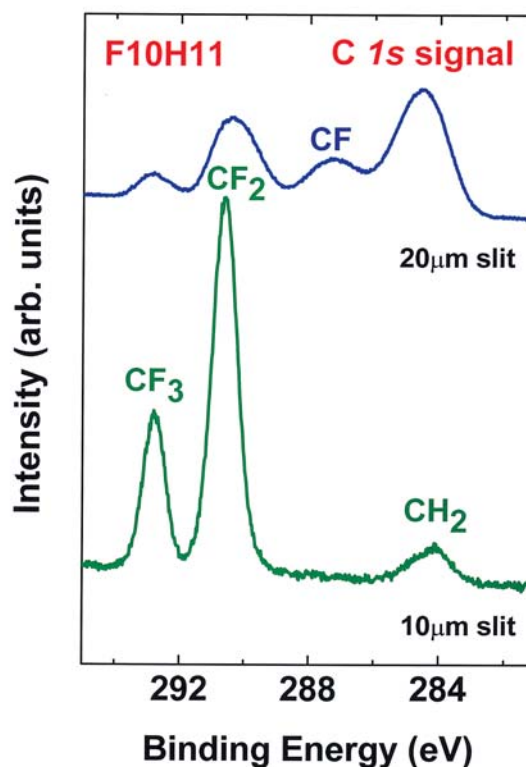


Fig. 2: C $1s$ photoemission spectra of F10H11/Au taken at a PE of 386 eV for different X-ray exposure. The exposure was set by selection of the exit slit of the beamline ($10 \mu\text{m}$, and $20 \mu\text{m}$, respectively) while the dwell time was kept fixed.

C $1s$ photoelectrons at a given kinetic energy (~ 100 eV) is only about 4 \AA . The spectrum drastically changed when the layer is exposed to a higher photon flux, as, e.g., provided by opening the exit slit of the beamline from 10 to $20 \mu\text{m}$. The intensities of the emissions related to the fluorocarbon part dramatically decrease, whereas a new emission at 287.3 eV appears, the signal at 284.1 eV increases, and all peaks become broader. Whereas the broadening is associated with a film disordering, the intensity changes originate from an extensive desorption of fluorocarbon species and fluorine, which results in a partial transformation of residual CF_2 and CF_3 entities to C-F moieties (a new peak at 287.3 eV) and to C-C/C=C species (an additional signal at the position of the CH_2 emission).

Therefore an especially high-contrast patterning could be achieved in F10H11/Au, as displayed in Fig. 3. The hydrocarbon-related image shows a particular strong enhancement in the intensity (73%) after the irradiation, which is noticeably

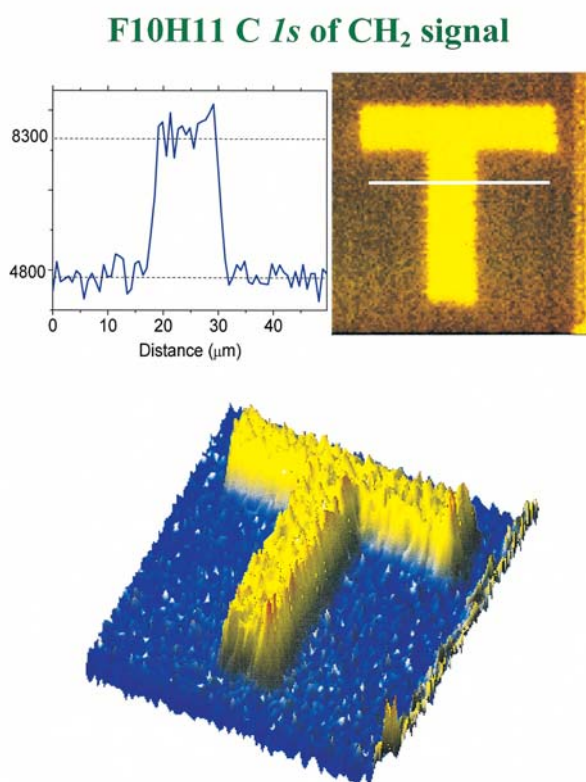


Fig. 3: Two- and three-dimensional C 1s (CH₂) SPEM images of soft X-ray microbeam patterned F10H11/Au taken at a PE of 387 eV (image size 70 × 70 μm²). Intensity profile taken along the line as indicated in the image. The image also contains contributions from the irradiation induced C-C and C=C moieties, which have a similar C 1s binding energy as CH₂ groups.

higher than the statistical noise in the image. Accordingly, the pristine/irradiated edge in the intensity profile is only slightly smeared by this noise and the spatial resolution can be estimated as $\approx 0.8 \mu\text{m}$, which correlates perfectly with the convolution of the pixel widths for the patterning ($0.5 \mu\text{m}$) and imaging ($0.7 \mu\text{m}$): $(0.5^2 + 0.7^2)^{1/2} = 0.86 \mu\text{m}$. The C 1s signal related to CF₂ species is weaker and the contrast is less pronounced.

Another example of soft X-ray lithography is given in Fig. 4, where the Au 4f images of two different patterns written in NBPT/Au are shown. It is clearly seen that the contrast is not as strong as in the case of the C16 and F10H11 resists (the respective C 1s contrast is even lower). Also, the intensity distribution within the X-ray-irradiated areas is rather inhomogeneous and the edges are blurred. This can be explained by a lower impact of the focused X-ray beam on the aromatic films

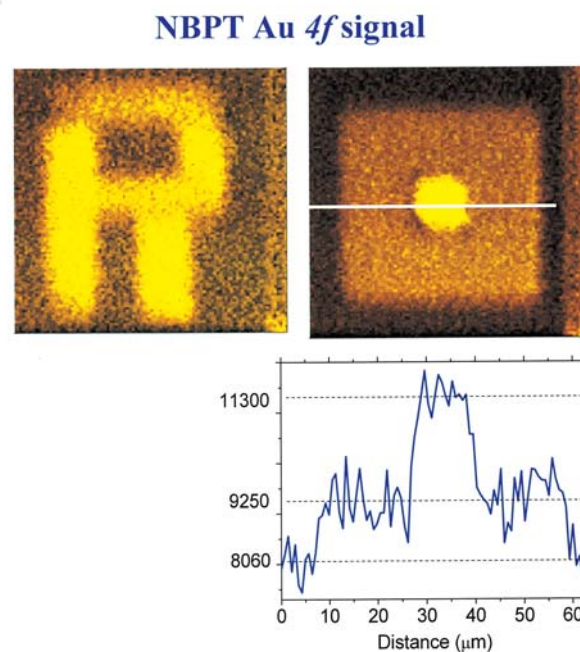


Fig. 4: Au 4f_{7/2} SPEM images (image size 70 × 70 μm²) of soft X-ray microbeam patterned NBPT/Au taken at a PE of 387 eV and intensity profile taken along the line as indicated in the image of a multi-exposure lithographic pattern (right image).

as compared to the aliphatic ones, similar to the case of electron beam irradiation. In addition, multi-exposure lithographic patterns were fabricated, as, e.g., displayed in the right part of Fig. 4 by the example of NBPT/Au. First, a small 10 × 10 μm² square was written with a pixel width of 200 nm and a dwell time of 160 ms (4 × 40 ms), followed by the writing of a larger 50 × 50 μm² square with a pixel size of 500 nm and a dwell time of 60 ms, and the imaging of the fabricated pattern with a pixel width of 700 nm and a dwell time of 60 ms. The intensity profile shows two steps of surface modification. As expected, the 10 μm inner square with the prolonged exposure time exhibits a stronger Au signal than other areas. The smaller pixel size and the longer dwell time result in a total X-ray exposure time which is about 9 times larger than that for the larger square. The respective increase in intensity is, however, only 22% while the intensity difference between the large square and the outer areas of the image is about 15%. The observed intensity relations correlate with a general evolution of the electron/X-ray induced modification of SAMs, which progresses rather fast at initial stages of irradiation and slows

down at a prolonged exposure.

The results show that soft X-ray lithography can be in principle used for an application-relevant patterning of a SAM resist. As for the experimental approach used in this study, its main advantages are a high flexibility and the possibility of simultaneous *in-situ* characterization of the fabricated patterns. In particular, chemical patterns can be produced and studied. Also, multi-exposure and gradient patterns can be fabricated, chemically modified (by letting suitable molecules into the SPEM chamber), and characterized within a single experiment.

Beamline:

09A1 U5/SPEM beamline

Experimental Station:

SPEM end station

Authors:

R. Klauser

National Synchrotron Radiation Research Center,
Hsinchu, Taiwan

M. Zharnikov

Angewandte Physikalische Chemie, Universität
Heidelberg, Heidelberg, Germany

Publications:

- R. Klauser, I.-H. Hong, T.-H. Lee, G.-C. Yin, D.-H. Wei, K.-L. Tsang, T. J. Chuang, S.-C. Wang, S. Gwo, M. Zharnikov, and J.-D. Liao, *Surf. Rev. Lett.* **9**, 213 (2002).
- M. Zharnikov, and M. Grunze, *J. Vac. Sci. Technol. B* **20**, 1793 (2002).
- R. Klauser, M. Zharnikov, I.-H. Hong, S.-C. Wang, A. Götzhäuser, and T. J. Chuang, *J. de Phys. IV* **104**, 459 (2003).
- R. Klauser, I.-H. Hong, S.-C. Wang, M. Zharnikov, A. Paul, A. Götzhäuser, A. Terfort, and T. J. Chuang, (submitted).
- R. Klauser, I.-H. Hong, M.-L. Huang, S.-C. Wang, T. J. Chuang, A. Terfort, and M. Zharnikov, (submitted).

Contact e-mail:

klauser@nsrrc.org.tw